Selective Two-Electron Oxygen Reduction for H_2O_2 Photosynthesis with Anthraquinone-Modified UiO-66/$Zn_3In_2S_6$ Heterojunctions

Jie Gao, [a] Chunsheng Ding, [a] Bonan Li, [a] Dian Zhang, [a] Lin Wang, [a] Xiaowen Ruan, [*a] Sai Kishore Ravi [*a]

[a] School of Energy and Environment, City University of Hong Kong, Tat Chee Avenue, Kowloon, Hong Kong SAR 999077, P.R. China.

* Represents the corresponding author

Corresponding Author: Sai Kishore Ravi; Xiaowen Ruan

E-mail: skravi@cityu.edu.hk; xiaoruan@cityu.edu.hk

Table of Contents

1. Chemicals and materials

Zinc sulphate heptahydrate ($ZnSO_4$•$7H_2O$, 99.995%), Indium trichloride tetrahydrate ($InCl_3$•$4H_2O$, 99.99%), Zirconium(IV) chloride ($ZrCl_4$, 99.5%), Terephthalic acid (PTA, 99%), Anthraquinone-2-carboxylic Acid (AQ, 98%), Acetonitrile (HPLC, 99.9%), para-benzoquinone (p-BQ, 99%), potassium iodide (KI, 99%), potassium hydrogen phthalate (99.8%) and N, N-dimethylformamide (DMF, 99.8%) were purchased from Aladdin Biochemical Technology Co., Ltd. Thioacetamide (TAA, 99%) was purchased from Meryer Technologies Co., Ltd. Tert-butyl alcohol (TBA, 99.5%), Manganese acetate dihydrate ($MnAC_3$, 97%), absolute ethanol were purchased from Macklin Biochemical Technology Co., Ltd. All the purchased chemicals can be used directly without any purification.

2. Synthesis of photocatalysts

2.1 Preparation of UiO-66 and UiO-66-AQ

First, 0.2 g of $ZrCl_4$ and 0.155 g of PTA were added to 50 mL of N, N-dimethylformamide (DMF), followed by the addition of 140 μL of deionized water. The mixture was stirred until completely dissolved and then transferred into a 100 mL Teflon-lined autoclave, where it was reacted at 120 °C for 24 h. After centrifugation, the resulting product was washed several times with deionized water and ethanol, and subsequently dried at 60 °C to obtain UiO-66.

To synthesize UiO-66-AQ, anthraquinone-2-carboxylic acid (AQ) and UiO-66 were mixed in various mass ratios using acetonitrile as the solvent. The mixture was stirred in an oil bath at 50 °C for 12 h. Following centrifugation and washing, the precipitates were dried at 60 °C to yield UiO-66 loaded with varying proportions of AQ (the UiO-66-AQ used in this study was synthesized via this method using 200 mg of UiO-66 and 100 mg of AQ).

2.2 Preparation of $Zn_3In_2S_6$

The preparation of $Zn_3In_2S_6$ was carried out according to previously reported literature. Specifically, 3 mmol of $ZnSO_4 \cdot 7H_2O$ and 2 mmol of $InCl_3 \cdot 4H_2O$ were added to 35 mL of deionized water. After stirring for 30 min, 12 mmol of thioacetamide

(TAA) was introduced, and the stirring was continued for another 30 min. Subsequently, the mixture was transferred into a 50 mL Teflon-lined autoclave and subjected to a hydrothermal reaction at 160 °C for 12 h. After cooling to room temperature, the obtained product was centrifuged and washed multiple times with deionized water and ethanol, and finally dried at 60°C to obtain $Zn_3In_2S_6$.

2.3 Preparation of $Zn_3In_2S_6$/UiO-66-AQ

The preparation of $Zn_3In_2S_6$/UiO-66-AQ was similar to that of $Zn_3In_2S_6$. The $Zn_3In_2S_6$ precursor solution was obtained following the same procedure described above. Subsequently, the pre-synthesized UiO-66-AQ was added to the $Zn_3In_2S_6$ precursor solution (the actual amount of UiO-66 added was adjusted based on the theoretical yield of $Zn_3In_2S_6$). The mixture underwent a hydrothermal reaction at 160 °C for 12 h to ensure the uniform loading of UiO-66-AQ onto the surface of $Zn_3In_2S_6$. The resulting product was centrifuged, washed several times with deionized water and ethanol, and then dried at 60 °C to yield the final $Zn_3In_2S_6$/UiO-66-AQ composite.

3. Characterization

The crystal structure is revealed by the powder X-ray diffraction (XRD) on a PANalytical X'Pert3 Powder diffractometer equipped with a Cu Kα source. A JEM-2000EX transmission electron microscope (JEOL Co, Japan) was used to acquire TEM images of the as-prepared samples with an acceleration voltage of 200 kV. The transmission electron microscopy (TEM) and high-resolution TEM (HRTEM) images were acquired by a JEOLJEM-2100F (UHR) Field Emission Transmission Electron Microscope. The surface morphology of the samples was characterized using scanning electron microscopy (SEM) on the QUATTROS equipment. The UV-visible absorption spectra of the samples were obtained by UV-vis spectrophotometer (PE Lambda 1050+). XPS was carried out to investigate the chemical states of the elements (Thermo Scientific K-Alpha, USA, with Al Kα radiation). In-situ XPS was conducted under otherwise identical conditions with ultraviolet irradiation. Time-resolved photoluminescence (TRPL) spectrum and Steady-state photoluminescence (PL) spectrum of the as-prepared samples were detected with an Edinburgh Instruments FS5

with a wavelength of 350 nm excitation. The surface potential distribution of the samples were characterized by Kelvin probe force microscopy (KPFM, Dimension Icon, Bruker). The electrochemical impedance spectra (EIS) analysis, transient photocurrent responses, linear sweep voltammetry curves (LSV) and open-circuit potential (OCP) transient decay curves were determined by using a CHI760F electrochemical workstation. Electron spin resonance (ESR) analysis was performed using electron spin resonance spectrometer (Jeol/JES-FA200). Fourier-transform infrared (FTIR) spectra were conducted on a Bruker INVENIO R infrared spectrophotometer.

4. Photocatalytic experiments and analysis

4.1 Photocatalytic H_2O_2 production

The photocatalytic generation of H_2O_2 was evaluated in pure water under ambient air, without the addition of any sacrificial agents. In a typical procedure, 5 mg of the photocatalyst was dispersed into 50 mL of pure water, and the reaction was immediately initiated by illuminating the suspension with a 300 W Xenon lamp (Perfect light, PLS-SXE300+/UV). Unless otherwise specified, the photocatalytic reactions were carried out at room temperature under ambient air in a 50 mL double-layer quartz glass reactor. The light source was operated at a current of 15 mA, covering a spectral range of 320–780 nm, with a total output power of 50 W. The concentration of the evolved H_2O_2 was determined using the iodometric method. Specifically, a 1 mL aliquot was sampled from the reactor and mixed with 1 mL of a 0.4 M aqueous potassium iodide (KI) solution and 1 mL of a 0.1 M aqueous potassium hydrogen phthalate solution. The absorbance of the resulting mixture was then measured at 350 nm using a UV-visible spectrophotometer. A standard calibration curve, prepared using commercial H_2O_2, was utilized for accurate quantification. Note: Unless stated otherwise, all photocatalytic H_2O_2 production experiments were conducted under an air atmosphere.

4.2 Photoelectrochemical measurements

Photoelectrochemical measurements were conducted on a CHI760F

electrochemical workstation utilizing a standard three-electrode cell configuration. In this setup, a Pt electrode served as the counter electrode, and an Ag/AgCl electrode was used as the reference electrode. The working electrode was prepared by dispersing 5 mg of the photocatalyst into 2 mL of a solvent mixture containing water, isopropanol, and Nafion solution (at a volume ratio of 1:1:0.025). This mixture was ultrasonicated for 30 min to yield a homogeneous slurry. The resulting suspension was then drop-cast onto a fluorine-doped tin oxide (FTO) glass substrate, with the active coating area carefully restricted to 1 cm^2. An aqueous 0.5 M Na_2SO_4 solution was employed as the electrolyte, and illumination was provided by a 300 W Xenon lamp.

4.3 The rotating ring disk electrode (RRDE) measurement

RRDE voltammetry was employed to investigate the ORR kinetics, specifically to quantify the transferred electron number (n) and H_2O_2 selectivity. Measurements were taken at 1600 rpm in an O_2-saturated phosphate buffer (pH = 7.0), with transferred electrons (n) derived from the formula below:

$$n = 4 \times \frac{I_d}{I_d + I_r/N}$$

The selectivity of H_2O_2 is calculated by the following formula:

$$H_2O_2\% = 2 \times \frac{I_r/N}{I_d + I_r/N} \times 100\%$$

where I_r is the ring current, I_d is the disk current, and N is the collection efficiency (N = 0.37).

4.4 Computational methods

All spin-polarized density functional theory (DFT) calculations were performed with the plane-wave basis set as implemented in the Vienna Ab Initio Simulation Package (VASP), and the electrons and ions interactions were described by the projector augmented wave (PAW) potential. The exchange–correlation interactions were determined by the Perdew–Burke–Ernzerhof (PBE) functional within the generalized gradient approximation (GGA). The plane wave energy cutoff of 500 eV, and the convergence criterion for the residual force and energy was set to 0.05 eV $Å^{-1}$ and 10^{-5} eV, respectively. The empirical correction in Grimme's method (DFT+D3)

was used to describe the van der Waals (vdW) interactions. The Brillouin region was sampled by the Monkhorst-Pack method with a 3×3×1 k-point mesh.

4.5 In-situ Fourier transform infrared (FTIR) Spectroscopy

After pressing the samples and loading them into the reaction chamber, high-purity helium was purged through the system for 30 min to desorb surface-bound impurities (e.g., H_2O, O_2, and CO_2). An initial infrared (IR) spectrum was immediately recorded to serve as the background baseline. Next, O_2 containing 5% water vapor was introduced at a flow rate of 40 $mL \cdot min^{-1}$. The system was kept in the dark for 30 min to allow for gas adsorption, during which the surface states were monitored via IR spectroscopy at 10-minute intervals. Following this dark adsorption phase, the chamber was sealed. A photocatalytic reaction was then triggered using full-spectrum irradiation for 30 min. Throughout this process, IR spectra were collected at predefined intervals over a wavenumber range of 4000 to 800 cm^{-1}.

5. Fig. S1-S17

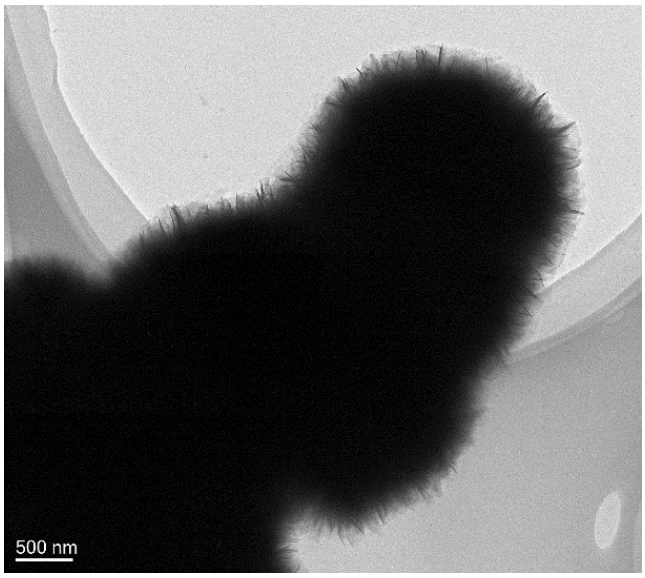

Figure S1. TEM image of $Zn_3In_2S_6$

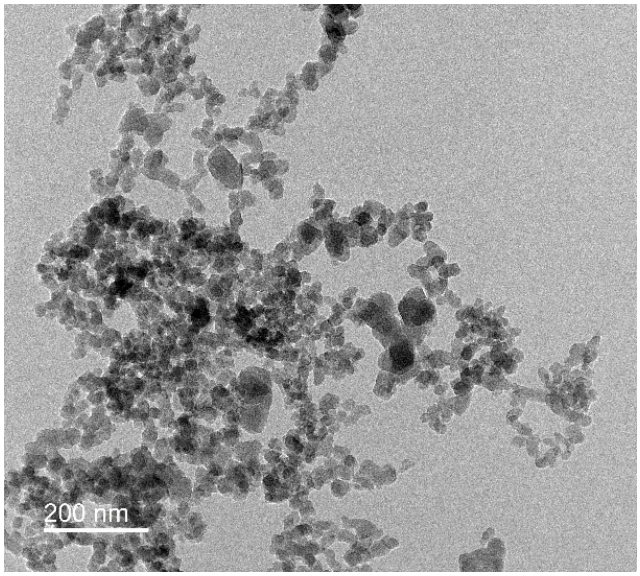

Figure S2. TEM image of UiO-66-AQ

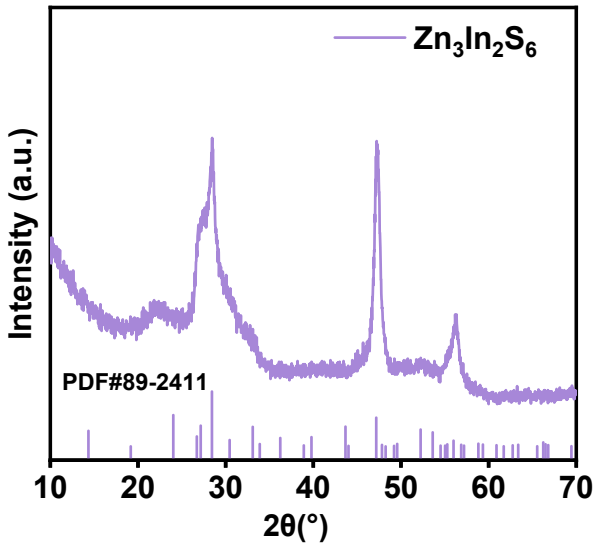

Figure S3. XRD pattern of as-prepared $Zn_3In_2S_6$

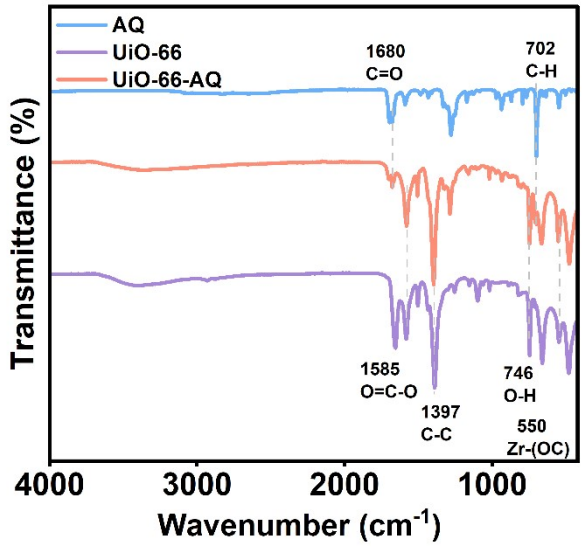

Figure S4. FTIR spectra of AQ, UiO-66 and UiO-66-AQ

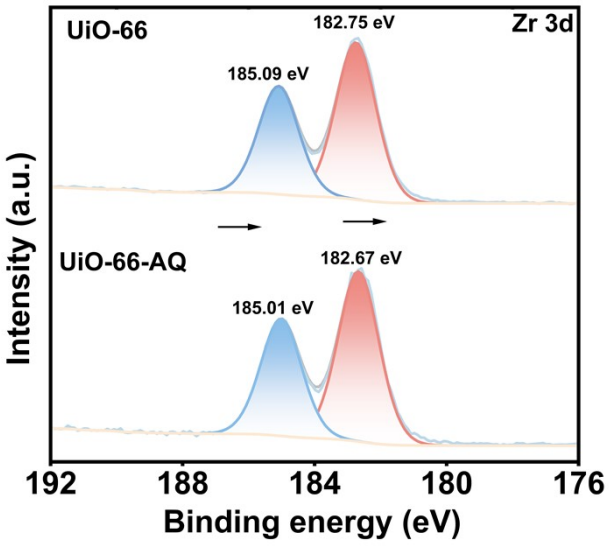

Figure S5. Zr 3d XPS spectra of UiO-66 and /UiO-66-AQ

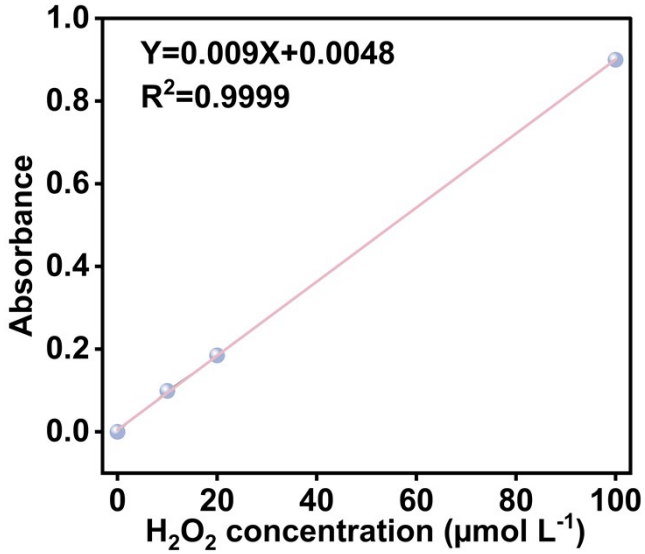

Figure S6. Calibration curve of H_2O_2 with standard concentrations

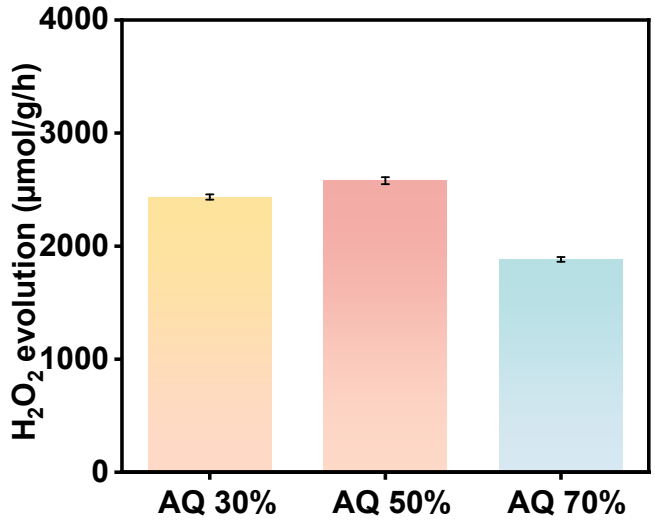

Figure S7. Hydrogen peroxide yield of UiO-66 with different loadings of anthraquinone-2-carboxylic acid

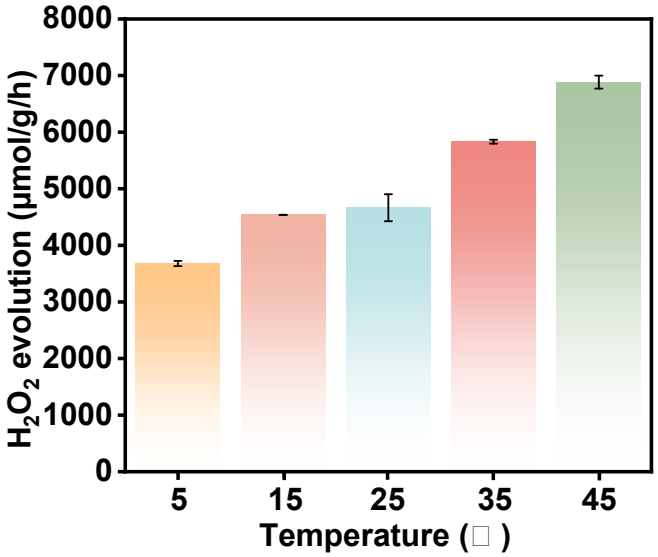

Figure S8. Hydrogen peroxide yield of $Zn_3In_2S_6$/UiO-66-AQ at different temperature

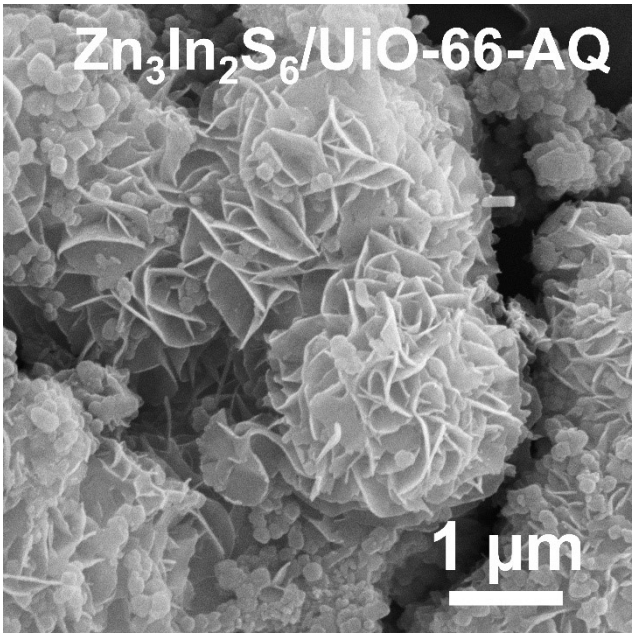

Figure S9. SEM images of $Zn_3In_2S_6$/UiO-66-AQ after photocatalytic tests.

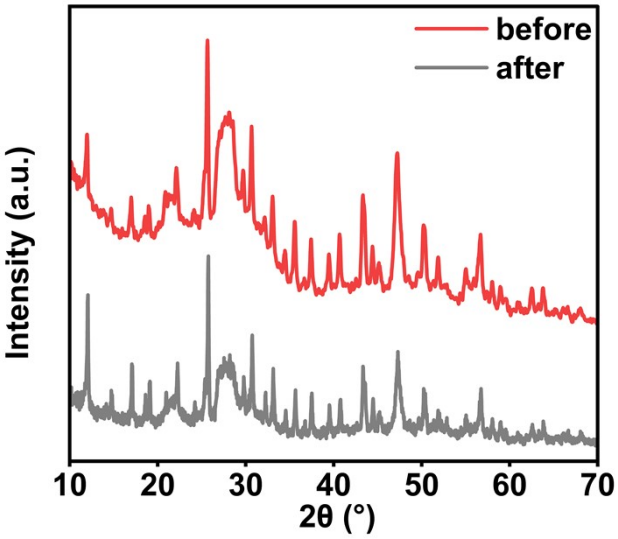

Figure S10. XRD patterns of $Zn_3In_2S_6$/UiO-66-AQ before and after photocatalytic tests.

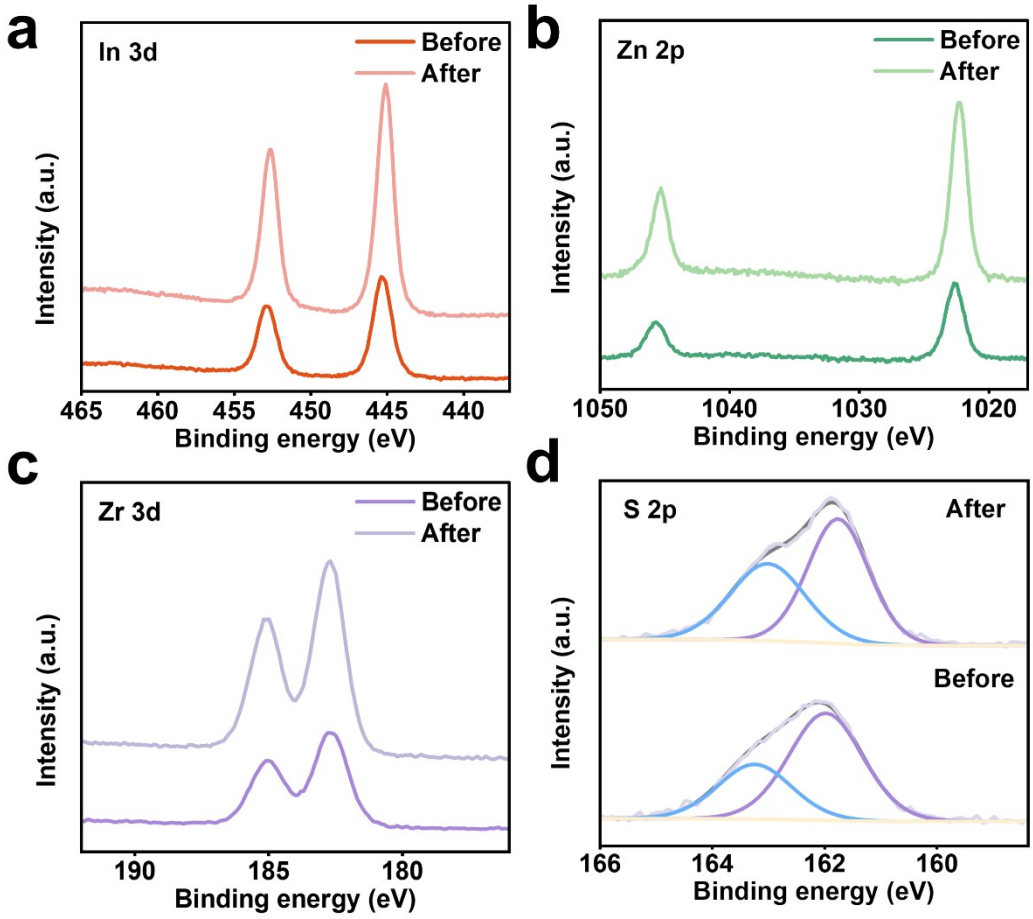

Figure S11. XPS spectra of $Zn_3In_2S_6$/UiO-66-AQ before and after the photocatalytic H_2O_2 evolution test**. (a)** In 3d, **(b)** Zn 2p, **(c)** Zr 3d and **(d)** S 2p

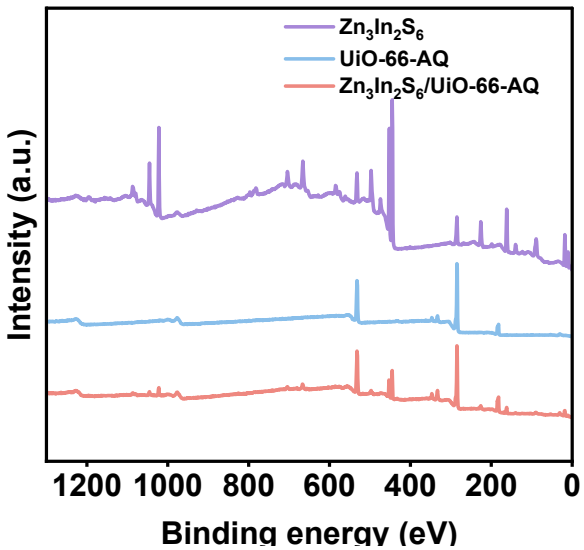

Figure S12. High-resolution XPS survey spectra of $Zn_3In_2S_6$, UiO-66-AQ and $Zn_3In_2S_6$/UiO-66-AQ

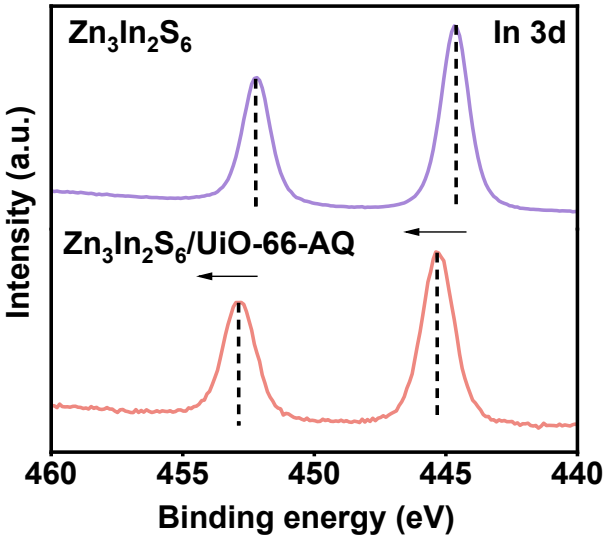

Figure S13. In 3d XPS spectra of $Zn_3In_2S_6$ and $Zn_3In_2S_6$/UiO-66-AQ

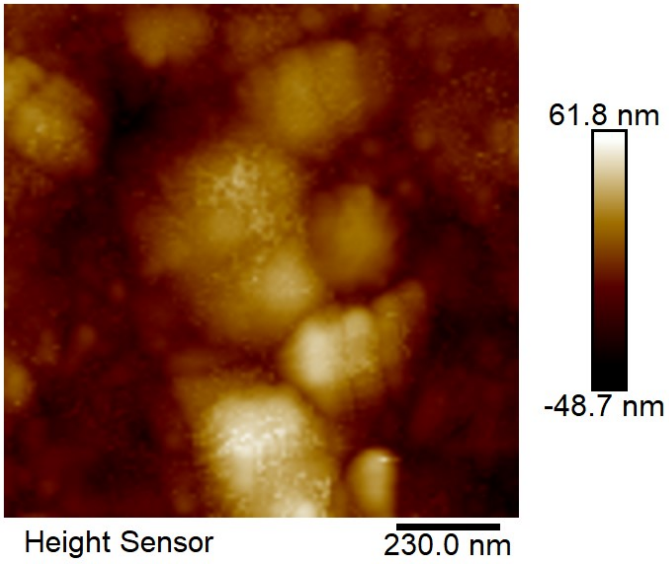

Figure S14. The height image of $Zn_3In_2S_6$

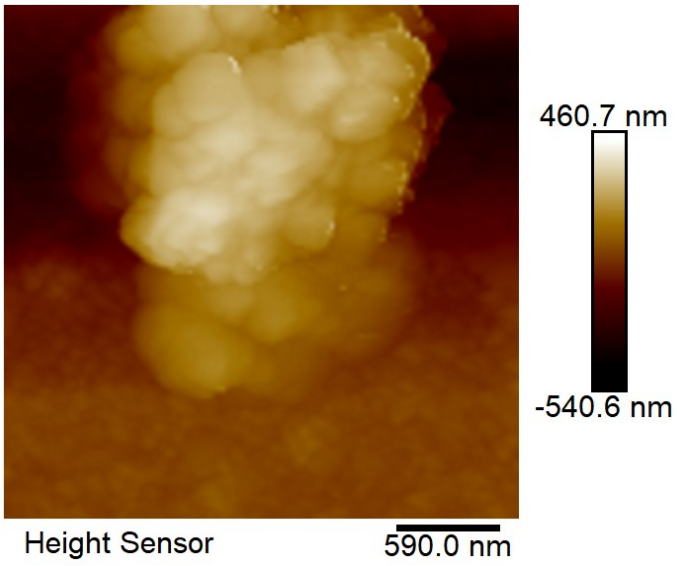

Figure S15. The height image of $Zn_3In_2S_6$/UiO-66-AQ

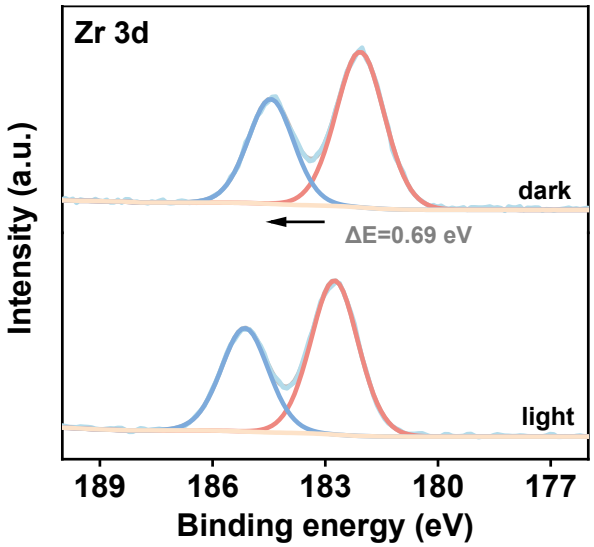

Figure S16. The in situ XPS spectra of Zr 3d

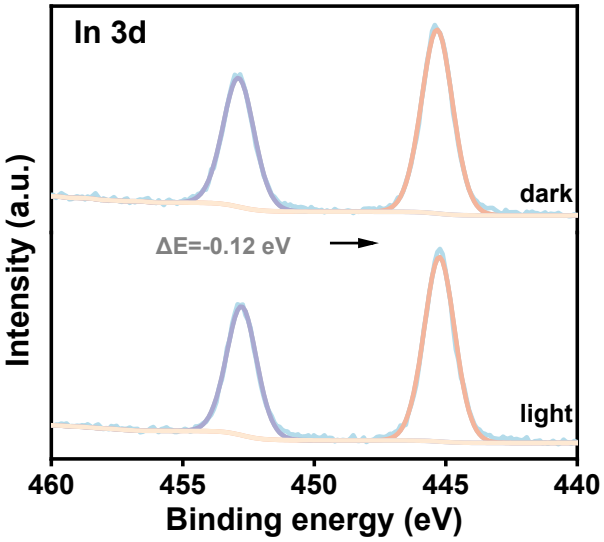

Figure S17. The in situ XPS spectra of In 3d

6. Table S1

Table S1. Comparison of the performance with other photocatalysts for photocatalytic production of H_2O_2

Catalysts	H_2O_2 evolution ($\mu mol\ g^{-1}\ h^{-1}$)	Catalyst mass (mg)	Reaction volume (mL)	Light source	Gas	Ref
$Zn_3In_2S_6$/UiO-66-AQ	4668	5 mg	50 mL	320 nm ≤ λ ≤ 780 nm	Air	This work
Cd-S_V/$Zn_3In_2S_6$	2365	10 mg	40 mL	UV–vis light	O_2	1
CN$ZnIn_2S_4$	1601	25 mg	50 mL	λ ≥ 420 nm	O_2	2
$ZnIn_2S_4$@$BiVO_4$	1800	10 mg	30 mL	400 nm ≤ λ ≤ 1000 nm	O_2	3
Sv- $ZnIn_2S_4$	1730	20 mg	30 mL	λ ≥ 400 nm	O_2	4
$ZnIn_2S_4$/$PDA_{0.1}$	1747	10 mg	50 mL	λ ≥ 420 nm	O_2	5
CdS@$ZnIn_2S_4$	605	15 mg	100 mL	λ > 400 nm	Ar	6
B20-$Zn_3In_2S_6$	3061	5 mg	52 mL	300 W xenon lamp	O_2	7
ZnO/UiO-66-NH_2	1185	20 mg	30 mL	λ = 365 nm	O_2	8
UiO-66-NH_2@ $ZnIn_2S_4$	3200	1 mg	10 mL	λ ≥ 400 nm	Air	9
chitosan-citric acid/NH_2-UiO-66	2668	50 mg	50 mL	300 W xenon lamp	Air	10
UiO-66-B	1002	30 mg	100 mL	AM 1.5	O_2	11
NH_2-UiO-66-50BA	250	20 mg	80 mL	λ > 420 nm	Air	12
Ni/Hf-UiO-66-NH_2	172.2	20 mg	10 mL	λ > 420 nm	O_2	13
UiO-66-NH_2/$Zn_{0.4}Cd_{0.6}S$-0.2	389.4	20 mg	40 mL	λ > 420 nm	Air	14
Pd_1/A-aUiO	1740	20 mg	50 mL	λ > 420 nm	O_2	15

All H_2O_2 production rates reported in this table were converted to the unified unit of $\mu mol\ g^{-1}\ h^{-1}$ for comparison. For values originally reported in $\mu mol\ g^{-1}\ min^{-1}$, the rates were multiplied by 60. For values reported in $\mu mol\ L^{-1}\ h^{-1}$, the rates were normalized by the reported reaction volume and catalyst mass according to R = C×V/m. The original experimental conditions were retained in the table.

References

1. D. Jiao, C. Ding, M. Xu, X. Ruan, S. K. Ravi and X. Cui, *Adv. Funct. Mater.*, 2025, **35**, 2416753.
2. K. Zhang, M. Dan, J. Yang, F. Wu, L. Wang, H. Tang and Z.-Q. Liu, *Adv. Funct. Mater.*, 2023, **33**, 2302964.
3. M. Gu, Y. Yang, L. Zhang, B. Zhu, G. Liang and J. Yu, *Applied Catalysis B: Environmental*,

2023, **324**, 122227.

4. H. Peng, H. Yang, J. Han, X. Liu, D. Su, T. Yang, S. Liu, C.-W. Pao, Z. Hu, Q. Zhang, Y. Xu, H. Geng and X. Huang, *J. Am. Chem. Soc.*, 2023, **145**, 27757-27766.
5. S. Huang, J. Gao, L. Zhou, J. Lei, L. Wang, Y. Liu and J. Zhang, *ACS Applied Nano Materials*, 2024, **7**, 4481-4490.
6. E. Zhang, Q. Zhu, J. Huang, J. Liu, G. Tan, C. Sun, T. Li, S. Liu, Y. Li, H. Wang, X. Wan, Z. Wen, F. Fan, J. Zhang and K. Ariga, *Applied Catalysis B: Environmental*, 2021, **293**, 120213.
7. J.-L. Zhou, Y.-F. Mu, M. Qiao, M.-R. Zhang, S.-X. Yuan, M. Zhang and T.-B. Lu, *Angew. Chem. Int. Ed.*, 2025, **64**, e202506963.
8. M. A. Qaiser, J. Li, W. Ren, S. Khan, S. B. Ahmed, W. A. Qureshi, M. H. Abdurahman, W. Wang and Q. Liu, *Chem. Eng. J.*, 2025, **525**, 170188.
9. Z. Gao, F. Liu, Z. Chen, Q. Song, P. J. Cullen, X. Zhang, Z. Zuo, J. Zhong, X. Lu, Z. Hu, R. Liu, Q. Zhang, Y. Yin and Y. Cai, *Nat. Commun.*, 2025, **16**, 8889.
10. Y. Lu, H. Zhu, Y. Han, Y. Tian, X. Liang, D. Nie, T. Ye, Y. Peng and X. Yang, *Chem. Eng. J.*, 2026, **535**, 175477.
11. Y. Li, F. Ma, L. Zheng, Y. Liu, Z. Wang, P. Wang, Z. Zheng, H. Cheng, Y. Dai and B. Huang, *Materials Horizons*, 2021, **8**, 2842-2850.
12. L. Li, X. Wang, H.-X. Liu, S.-S. Xia, Z. Chen and J. Ye, *J. Catal.*, 2024, **429**, 115249.
13. Y. Kondo, K. Honda, Y. Kuwahara, K. Mori, H. Kobayashi and H. Yamashita, *ACS Catalysis*, 2022, **12**, 14825-14835.
14. W. Chen, S.-Z. Lin, Z. Song, G.-B. Huang and M. Zhang, *Journal of Materials Science & Technology*, 2025, **232**, 246-256.
15. Y.-C. Hao, L.-W. Chen, J. Li, Y. Guo, X. Su, M. Shu, Q. Zhang, W.-Y. Gao, S. Li, Z.-L. Yu, L. Gu, X. Feng, A.-X. Yin, R. Si, Y.-W. Zhang, B. Wang and C.-H. Yan, *Nat. Commun.*, 2021, **12**, 2682.